JOURNAL OF OPTOELECTRONICS AND ADVANCED MATERIALS, Vol. 11, No. 5, May 2009, p. 578 - 582

Numerical optimization of Al-mole fractions and layer thicknesses in normally-on AlGaN-GaN double-channel high electron mobility transistors (DCHEMTs)

G. ATMACA, K. ELIBOL, S. B. LISESIVDIN[a]*, M. KASAP, E. OZBAY[a,b]
Department of Physics, Faculty of Science and Arts, Gazi University, Teknikokullar, 06500 Ankara, Turkey
[a]Nanotechnology Research Center, Bilkent University, Bilkent, 06800 Ankara, Turkey
[b]Department of Physics, Bilkent University, Bilkent, 06800 Ankara, Turkey; and Department of Electrical and Electronics Engineering, Bilkent University, Bilkent, 06800 Ankara, Turkey.

We explored the effects of the Al-mole fraction (x) of $Al_xGa_{1-x}N$ barrier layers and the thickness of some layers on carrier densities and electron probability densities in normally-on AlGaN-GaN double-channel high electron mobility transistors. Investigations were carried out by solving non-linear Schrödinger-Poisson equations, self-consistently including polarization induced carriers that are important for GaN-based heterostructures and two-dimensional electron gas (2DEG) formation. Strain relaxation limits were also calculated, in which optimized cases were found for the investigated Al-mole fraction and thickness values under pseudomorphic limits. The effect of the investigated thickness changes on electron probability densities show no important change in the overall simulations. In addition to a carrier increase in the selected optimum cases, reasonable mobility behavior is also expected.

(Received April 15, 2009; accepted May 25, 2009)

Keywords: AlGaN, DCHEMT, HEMT, Schrödinger, Poisson, 2DEG

1. Introduction

GaN-based high electron mobility transistors (HEMTs) have demonstrated a large potential for applications in high–power, –frequency, and –temperature electronics [1-3]. Significant improvements in rf and dc performances have been achieved with improvements in material quality, device fabrication, and layer structures [4-7]. However, in spite of the improvements made, GaN-based HEMTs are still far from reaching the theoretical maximum performances. In GaN-based heterostructures - including HEMTs - with wurtzite crystal structures in the 0001 orientation, there are strong polarization fields. These polarization fields are classified as the piezoelectric polarization field [8] and spontaneous (or pyroelectric) polarization field [9], in which these fields largely influence the band structures and electron densities of these heterostructures. Further investigation and understanding of the transport properties of the polarization-induced two-dimensional electron gas (2DEG) is required for the improvement of the device performances.

To explore further improvements in device performance, double-channel HEMTs (DCHEMTs) have been reported for reduced access resistance and improved linearity [10, 11]. Further improvements in transport properties such as the carrier densities and mobilities of 2DEG are also reported. The effect of polarization is known to be enhanced in DCHEMTs, compared to conventional HEMTs. In DCHEMTs, both positive and negative polarization charges emerge at the 2DEG interfaces. In a conventional GaN-based HEMT, only positive polarization emerges at the 2DEG interface. Therefore, the total electric field is increased in DCHEMT structures, which concludes an important carrier density increase [10]. This phenomenon is specific to nitride heterostructures where the large polarization fields exist. Maeda *et al.* observed drastically enhanced 2DEG mobility in DCHEMTs compared with that in HEMTs, for those samples with carrier densities of approx. 7×10^{12} cm^{-2} [12]. Because of these advantages attained by the structure, interest in GaN-based DCHEMTs has grown recently [7, 13-15].

In the present study, we theoretically explore the effects of the Al-mole fraction (x) of $Al_xGa_{1-x}N$ layers and the layer thicknesses of some layers on the carrier densities and electron probability densities in normally-on AlGaN-GaN-based DCHEMT structures. Investigations were carried out by solving non-linear Schrödinger-Poisson equations, self-consistently including polarization induced carriers was calculated using *next*nano^3 device simulation package for the wurtzite 0001 growth axis [16]. The strain relaxation limits were also calculated with a simple critical thickness calculation approach [17].

2. Device structures and simulation

Fig. 1 shows the layer sequence of the simulated DCHEMT structures. All of the layers are grown on a GaN buffer pseudomorphically. From the buffer to cap

layer, which are two channels that are hereinafter referred to as α-well and β-well, are presumed to be observed. AlN interlayers are used with thicknesses of 1 nm, which is well known to be the optimum thickness value for higher mobility and carrier density [17, 18]. In the simulations, the Al-mole fraction of $Al_xGa_{1-x}N$ layers, the thickness of the $Al_xGa_{1-x}N$ layer of □-well and the thickness of the GaN layer of β-well are changed systematically, and their effects on the carrier densities and electron probability densities are investigated.

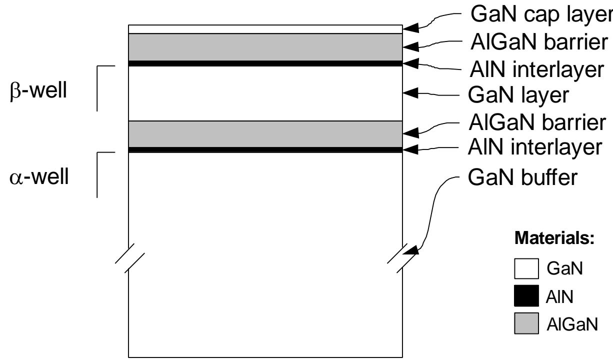

Fig. 1. Simulated device structure.

Every simulation procedure begins with a strain calculation with homogeneous strain dispersion over the simulated region. The strain tensor ε, which is the symmetrical part of the deformation tensor can be defined as

$$\varepsilon_{ij} = \frac{\vec{u}_{ij} + \vec{u}_{ji}}{2} = \varepsilon_{ji} \,. \qquad (1)$$

Here, $\vec{u}$ is the displacement due to lattice deformations and *i,j = {1,2,3}*. The off-diagonal strain components (shear strain) measure the strain where the angles change and the volume remains constant. For the 0001 growth axis wurtzite structure, the off-diagonal strain components are all accepted as zero ($\varepsilon_{xy} = \varepsilon_{xz} = \varepsilon_{yz} = 0$). Diagonal strain components are related with the volume change in crystal. For the 0001 growth axis wurtzite structure, diagonal strain components ($\varepsilon_{xx}, \varepsilon_{yy}, \varepsilon_{zz}$) are related with each other and can be easily calculated from the lattice parameters of the related layers as follows

$$\varepsilon_{xx} = \varepsilon_{yy} = \frac{a_{Bottom} - a_{Upper}}{a_{Upper}} \qquad (2)$$

$$\varepsilon_{zz} = -2(C_{13} / C_{33})\varepsilon_{xx} \qquad (3)$$

Here, C_{11} and C_{33} are the elastic constants, a_{Bottom} and a_{Upper} are the lattice parameters of the bottom and related upper layers, respectively. ε_{xx} and ε_{yy} are called bi-axial strain, and they are in plane of interface where the strain formed. ε_{zz} is called uni-axial strain and it is perpendicular to interface. After strain calculation, the band edges are calculated by taking full account of the van-de-Walle model and strain. With the calculated strain, the piezoelectric polarization of each layer are then calculated with using

$$P_{PE} = 2\varepsilon_{xx}\left\{ e_{31} - e_{33}\frac{C_{13}}{C_{33}} \right\} \quad C/m^2 \,. \qquad (4)$$

Here, e_{31} and e_{33} are the piezoelectric constants. The spatial variation of total polarization leads to polarization induced carriers. With the known spontaneous polarization (P_{SP}) and the calculated piezoelectric polarizations of the related layers, polarization induced charge densities are calculated.

Table 1. Lattice parameters, elastic constants, piezoelectric constants and the spontaneous polarization values of GaN and AlN materials [19-22].

Parameter	GaN	AlN
a (nm)	0.3189	0.3112
e_{31} (C/m^2)	-0.35	-0.50
e_{33} (C/m^2)	1.27	1.79
C_{13} (GPa)	106	108
C_{33} (GPa)	398	373
P_{SP} (C/m^2)	-0.034	-0.090

The quantum states are allocated in previously determined quantum regions. Subsequently, a starting potential value is determined and the nonlinear Poisson equation is solved with the calculated piezoelectric and spontaneous charges. In the last step of the simulation, Schrödinger's equation and Poisson's equation are both solved self-consistently in order to obtain the carrier distribution, wave functions, and related eigenenergies. The material parameters i.e. lattice parameters, elastic constants, piezoelectric constants and the spontaneous polarization values of AlN and GaN, are listed in Table 1 [19-22]. For the $Al_xGa_{1-x}N$ layers, lattice parameters, elastic constants and piezoelectric constants are calculated with Vegard's law. For the spontaneous polarization of $Al_xGa_{1-x}N$ layers, following bowing formula is used [19]

$$P_{SP}^{Al_xGa_{1-x}N} = xP_{SP}^{AlN} + (1-x)P_{SP}^{GaN} + 0.021x(1-x) \qquad (5)$$

The conduction band structures, electron densities, and wave functions of the electrons are calculated for different layer thicknesses and different Al-mole fractions. In every case, the strain values are calculated. A simple estimation for the critical thickness below the strain relaxation limit is given by the relation [17] : $t_{cr} \cong b_e / \varepsilon_{xx}$. Here, b_e is the Burger's vector with a value

of b_e = 0.31825 nm [23]. We assume a total homogeneous strain over the GaN layers of the each pseudotriangular quantum well, which is calculated with the strain values of every layer over the related GaN layer.

3. Results and discussion

Fig. 2 shows the calculated conduction band energy diagram for the case of $t_{\alpha\text{-}AlGaN}$ = 10 nm, $t_{\beta\text{-}AlGaN}$ = 25 nm, $t_{\beta\text{-}GaN}$ = 25 nm, and x = 0.25, as an example. Here, t represents the related layer thicknesses. For the case shown in the figure, the first eigenvalues of both wells are under the Fermi level, which means both wells are populated. To find an optimum result, we firstly investigated the effect of the $Al_xGa_{1-x}N$ barrier layer thickness of α-well on the carrier densities.

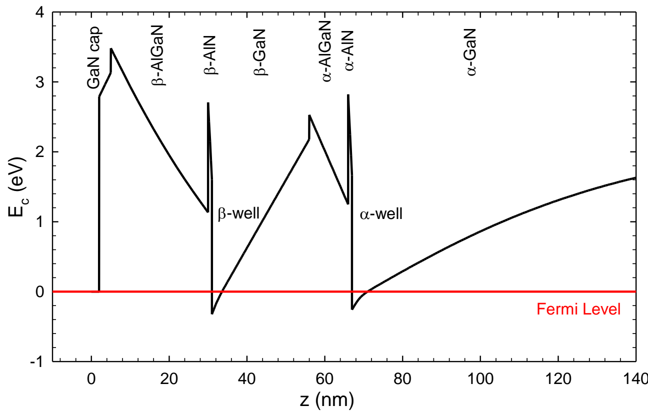

Fig. 2 Calculated conduction band energy (E_C) diagram for a DCHEMT structure. Layers are shown with a material name that has a well name prefix.

Fig. 3 (a) shows the $t_{\alpha\text{-}AlGaN}$ dependent total carrier densities for the cases x = 0.25, 0.35, and 0.45. Here, the β-GaN thickness is accepted as 25 nm, which is under strain relaxation for a single channel HEMT case. As can be seen in the figure, generally, carrier densities increase with the increase of t□-AlGaN values. This behavior is typical for conventional HEMT structures [24]. In our case, carrier densities are intended to increase due to the populated second channel at low thickness values. In the figure, the pseudomorphic cases are shown as solid lines and the values above the strain relaxation are shown as dashed lines. The highest carrier density increase in the pseudomorphic cases was observed for x = 0.25. In order to investigate the effect of a second conducting channel, the individual carrier densities of both wells are shown in Fig. 3 (b). The barrier thickness dependent behavior of the carrier densities of α-well is typical for a conventional HEMT structure, as stated above. The carrier density of β-well decreases along with the increase of $t_{\alpha\text{-}AlGaN}$. This behavior is due to the increased band offset between the wells that cause a depopulation of β-well.

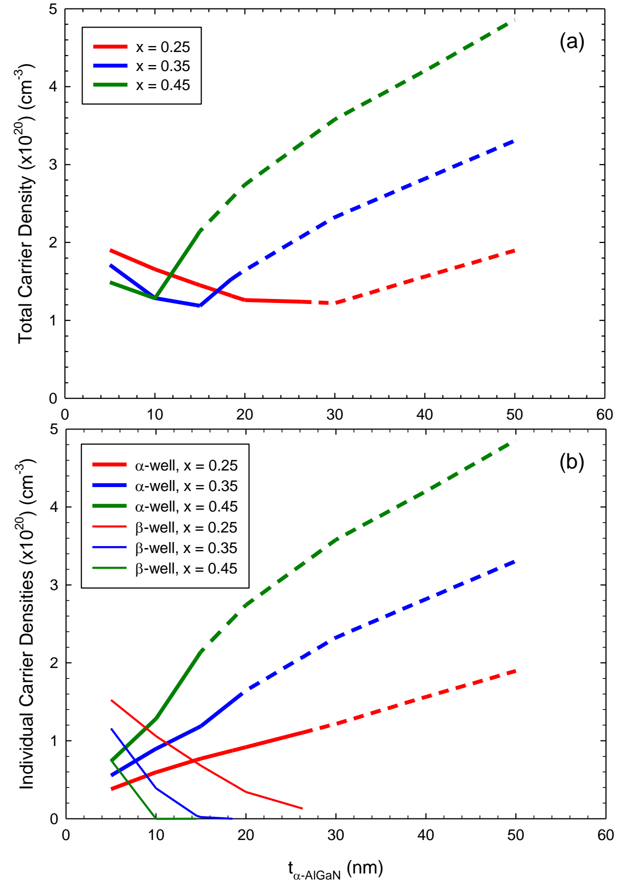

Fig. 3 (a) α-AlGaN barrier thickness dependent total carrier densities of both wells and (b) individual carrier densities of both wells for different Al-mole fractions. Dashed lines represent the strain relaxed situation.

Fig. 4 (a) and (b) show the wavefunctions of the 2DEG carriers of α-well and β-well, respectively. As can be seen in the figure, the probability densities of the carriers are nearly independent of the $t_{\alpha\text{-}AlGaN}$ change. If we accept that the probability densities of the carriers are linearly correlated with the well-width of the pseudotriangular quantum wells, then we can conclude that all of the well-width dependent scattering mechanisms such as background impurity (BI) scattering ($\mu_{BI} \propto Z_0^{-1}$) [25], interface roughness (IFR) scattering ($\mu_{IFR} \propto Z_0^{6}$) [26, 27], and polar optical phonon (PO) scattering ($\mu_{PO} \propto Z_0^{-1}$) [28] are not significantly changed with the $t_{\alpha\text{-}AlGaN}$. For 2D carriers, IFR and PO are the dominant scattering mechanism at low temperatures [29] and [28] at high temperatures, respectively. In order to find an optimum result, we accepted a thickness of $t_{\alpha\text{-}AlGaN}$ = 10 nm. For this thickness value, the total carrier density of the DCHEMT structure was 150% greater than a conventional HEMT structure with a barrier thickness of 25 nm (just below strain relaxation). In addition to the increase in the carrier density, the mobility behaviors of the 2DEG carriers of both wells were also expected to be reasonable.

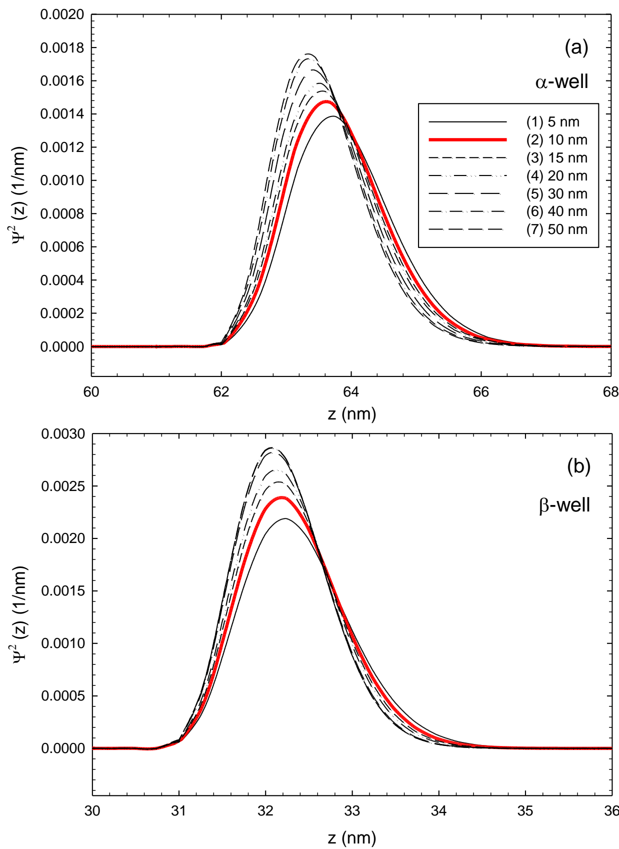

Fig. 4 Probability densities of the 2DEG carriers of (a) α-well and (b) β-well for different $t_{\alpha\text{-}AlGaN}$ values.

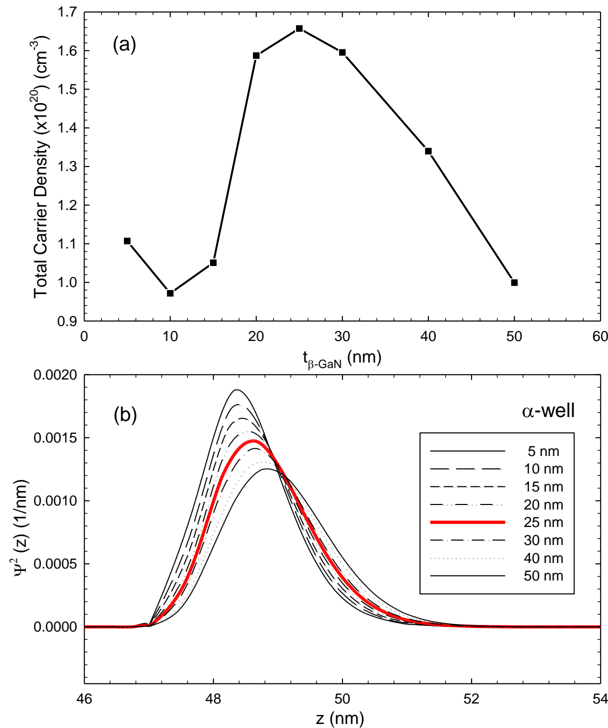

Fig. 5 (a) β-GaN thickness dependent total carrier densities of both wells and (b) probability densities of the 2DEG carriers of α-well for different $t_{\beta\text{-}GaN}$ values.

Fig. 5 (a) shows the total carrier density versus the β-GaN thickness ($t_{\beta\text{-}GaN}$) results. The total carrier density was decreased drastically for $t_{\beta\text{-}GaN} < 20$ nm due to the depopulation of β-well. The maximum carrier density was calculated for the $t_{\beta\text{-}GaN} = 25$ nm case. Fig. 5 (b) shows the wavefunctions of the 2DEG carriers of α-well for different $t_{\beta\text{-}GaN}$ values. In this case, the behavior of β-well is nearly the same as α-well. The wavefunction of the 2DEG carriers of the $t_{\beta\text{-}GaN} = 25$ nm case is not near to the AlN/GaN interface and does not broaden into the GaN layer. It can be concluded that the $t_{\beta\text{-}GaN} = 25$ nm case can be accepted as an optimum case with a reasonable response to scattering mechanisms as discussed above and with the observed maximum total carrier density values.

4. Conclusions

We have modeled the effects of the Al-mole fraction of $Al_xGa_{1-x}N$ barrier layers and the thickness of some layers on the carrier densities and electron probability densities of both pseudotriangular quantum wells in normally-on AlGaN-GaN based DCHEMT structures with self-consistent solutions of non-linear Schrödinger-Poisson equations. The well near the substrate is called alpha and the other is beta, in which all of the related layers to the corresponding well are prefixed with these names. The pseudomorphic conditions were also calculated for all the simulations, in which the optimizations were limited within the strain relaxation limits. The highest increases in the total carrier density were calculated for $x = 0.25$. Here, $t_{\square\text{-}AlGaN}$ was used as 25 nm and the AlN interlayers were used as 1 nm each. The effects of the thicknesses of α-AlGaN and β-GaN on the electron probability densities shows no important change so that the $t_{\square\text{-}AlGaN} = 10$ nm and $t_{\square\text{-}GaN} = 25$ nm values are accepted as optimized values due to the important increase in the carrier densities in these respective thicknesses values.

These simulation results are important figures of merit in order to experimentally obtain higher carrier densities in normally-on DCHEMT structures. Future experimental explorations involving pseudomorphic growths could cast a definitive answer in terms of carrier density and mobility, which is, however, beyond the scope of the present paper.

Acknowledgements

This work is supported by the European Union under the projects EU-PHOME, and EU-ECONAM, and TUBITAK under Project Nos. 106E198, 107A004, and 107A012. One of the authors (E.O.) also acknowledges partial support from the Turkish Academy of Sciences.

References

[1] M. S. Shur, Solid State Electron. **42**, 2131 (1998).

[2] A. Christou, Physica B **296**, 264 (2001).
[3] E. Waki, T. Deguchi, A. Nakagawa, T. Egawa, Appl. Phys. Lett. **92**, 103507 (2008).
[4] I. P. Smorchkova, S. Keller, S. Heikman, C. R. Elsass, B. Heying, P. Fini, J. S. Speck, U. K. Mishra, Appl. Phys. Lett. **77**, 3998 (2000).
[5] O. Ambacher, B. Foutz, J. Smart, J. R. Shealy, N. G. Weimann, K. Chu, M. Murphy, A. J. Sierakowski, W. J. Schaff, L. F. Eastman, J. Appl. Phys. **87**, 334 (2000).
[6] Y. F. Wu, A. Saxler, M. Moore, R. P. Smith, S. Sheppard, P. M. Chavarkar T. Wisleder, U. K. Mishra, P. Parikh, IEEE Electron Device Lett. **25**, 117 (2004).
[7] T. Palacios, A. Chakraborty, S. Keller, S. P. DenBaars, U. K. Mishra, IEEE Electron Device Lett. **27**, 13 (2006).
[8] A. Bykhovski, B. Gelmont, M. Shur, J. Appl. Phys. **74**, 6734 (1993).
[9] F. Bernardini, V. Fiorentini, Phys. Rev B **56**, 10024 (1997).
[10] N. Maeda, T. Saitoh, K. Tsubaki, T. Nishida, N. Kobayashi, Appl. Phys. Lett. **76**, 3118 (2000).
[11] T. Palacios, A. Chini, D. Buttari, S. Heikman, A. Chakraborty, S. Keller, S. P. DenBaar, U. K. Mishra, IEEE T. Electron Dev. **53**, 562 (2006).
[12] N. Maeda, T. Saitoh, K. Tsubaki, T. Nishida, N. Kobayashi, Jpn. J. Appl. Phys. **38**, L799 (1999).
[13] S. K. Jha, C. Surya, K. J. Chen, K. M. Lau, E. Jelencovic, Solid State Electron. **52**, 606 (2008).
[14] J. Y. Zheng, J. S. Wu, D. R. Lin, and H. J. Lin, Phys. Stat. Sol. (c) **5**, 1944 (2008).
[15] A. Vescan, H. Hardtdegen, N. Ketteniss, M. Eickelkamp, A. Noculak, J. Goliasch, M. v.d. Ahe, H. L. Bay, T. Schäpers, H. Kalisch, D. Grützmacher, R. H. Jansen, Phys. Stat. Sol. (c) (DOI 10.1002/pssc.200880855) (2009).
[16] S. Birner, S. Hackenbuchner, M. Sabathil, G. Zandler, J. A. Majewski, T. Andlauer, T. Zibold, R. Morschl, A. Trellakis, P. Vogl, Acta Phys. Pol. A **110,** 111 (2006).
[17] M. Gonscherek, J. -F. Carlin, E. Feltin, M. A. Py, N. Grandjean, V. Darakchieva, B. Monemar, M. Lorenz, and G. Ramm, J. Appl. Phys. **103**, 093714 (2008).
[18] S. B. Lisesivdin, A. Yildiz, M. Kasap, Optoelectron. Adv. Mater. - Rapid Comm. **1**, 467 (2007).
[19] I. Vurgaftman, J. R. Meyer J. Appl. Phys. **96,** 3675 (2003).
[20] I. Vurgaftman, J. R. Meyer, L. R. Ram-Mohan J. Appl. Phys. **89** 5815 (2001).
[21] O. Ambacher, J. Majewski, C. Miskys, A. Link, M. Hermann, M. Eickhoff, M. Stutzmann, F. Bernardini, V. Fiorentini, V. Tilak, B. Schaff, L. F. Eastman, J. Phys.: Condens. Matter **14,** 3399 (2002).
[22] H. Morkoç "Nitride Semiconductors and Devices" Springer-Verlag, Berlin Heidelberg (1999).
[23] J. Singh, "Physics of Semiconductors and Their Heterostructures" McGraw-Hill, New York, (1992), p. 734.
[24] L. Hsu, W. Walukiewicz, J. Appl. Phys. **89**, 1783 (2001).
[25] K. Hess, Appl. Phys. Lett **35**, 484 (1979).
[26] H. Sakaki, T. Noda, K. Hirakawa, M. Tanaka, T. Matsusue, Appl. Phys. Lett. **51**, 1934 (1987).
[27] J. M. Li, J. J. Wu, X. X. Han, Y. W. Lu, X. L. Liu, Q. S. Zhu, Z. G. Wang, Semicond. Sci. Technol. **20**, 1207 (2005).
[28] B. K. Ridley, J. Phys. C: Solid State Phys **15**, 5899 (1982).
[29] D. Zanato, S. Gokden, N. Balkan, B. K. Ridley, W. J. Schaff, Semicond. Sci. Technol. **19**, 427 (2004).

*Corresponding author: sblisesivdin@gmail.com